International Journal of Materials Engineering 2015, 5(5): 113-120
DOI: 10.5923/j.ijme.20150505.02

Effect of Fiber YAG Laser Parameters on the Microstructural and Mechanical Properties of High Strength Low Alloy Steel

Ali Algahtani[1,*], Essam R. I. Mahmoud[2]

[1]Faculty of Engineering, King Khalid University, Abha, Kingdom of Saudi Arabia
[2]Central Metallurgical Research and Development Institute, Cairo, Egypt

Abstract This article reports on an experimental investigation to weld high strength low alloy steel using YAG fiber laser at different processing conditions. Three level of the laser power were investigated: 2500 W, 2000 W and 1500 W, at fixed welding speed of 40 mm/s. Welding speeds of 50 mm/s, 40 mm/s and 25 mm/s were used at a fixed power of 2500 W. Moreover, the defocusing distance was changed from -2 mm to +1.5 mm at a fixed power of 2500 W and speed of 40 mm/s. Full penetration joints without any macro defects were produced by laser power more than 2000 W. While at 1500 W, partial penetration defect was occurred. The microstructure of the weld zone show acicular ferrite and bainite at higher power and martensite and some ferrite at lower power. When the laser speed was decreased to 25 mm/s, the width of the weld and heat affected zone became wide. Lack of penetration and other defects (porosity) with wide weld zone were appeared at defocusing distance more than -1 mm. The welded joints that welded with higher laser powers and negative defocusing distance gave fracture strength values very close to that of the base metal

Keywords HSLA steel, Laser welding, Laser power, Laser speed

1. Introduction

In recent past, the demand of environment-friendly vehicles that have better fuel economy and lower CO2 emissions compels automakers to apply advanced technology and new materials in vehicle manufacturing [1–3]. Moreover, the increasing length of bridges, shipbuilding, and oil & gas transmission pipelines associated with their construction and operating costs has lead to the development of a new steel grades with light weight and higher performance [4-6]. To achieve these objectives, high strength low alloy (HSLA) steels can be used in all these applications. HSLA steels are high potential materials for light structures where considerable strength is required [7-8]. The combination of strength, toughness, formability and better performance both in high and low temperature enables construction engineers to use HSLA steel alloys with thinner thickness in many industrial applications [9]. During manufacturing of all these components, welding and joining are unavoidable. Many welding techniques such as metal inert gas/active gas (MIG/MAG) welding, tungsten inert gas (TIG) welding or other arc welding methods have been used for many years [10-11].

The studies showed that these traditional methods have disadvantages of higher heat input generated which leads to problems such as as lager fusion and heat-affected zones, coarse grains, bigger deformations and more defects such as cracks and porosity in addition to low productivity [12-14].

It is therefore advantageous to develop welding process that minimize heat input and maintain the fine grain structure that provides the strength and toughness. Low heat input welding operations also have the extra benefit of decreasing welding induced distortion [15-16]. Correcting distortion may require mechanical and/or thermal methods such as flame straightening operations which, if not carefully controlled, could also lead to grain growth and degradation of the mechanical properties. As such, laser welding has been given great expectations to solve these problems, as it has high welding speed, deep penetration, narrow bead width and low distortion [17]. A new generation of fiber lasers has been developed for industrial applications and has multiple advantages, including high power with small beam divergence, flexible beam delivery, low maintenance costs, high efficiency, compact size and ease of interface with robots [15-18]. Nd:YAG laser welding is becoming increasingly important and its share in the total laser industry is expected to grow substantially [19]. One of the reasons is that the high power density, lower maintenance costs, small beam divergence and focal spot diameter could lead to welds

* Corresponding author:
alialgahtani@kku.edu.sa (Ali Algahtani)
Published online at http://journal.sapub.org/ijme

with a higher penetration and smaller width for a given welding speed [19]. During the process of laser beam welding, many factors, such as laser power, welding speed, focus position, work piece distortion and surface condition, influence the absorption rate of laser energy, and then the weld quality may be changed. In order to ensure good weld quality, the process control should be conducted during laser beam welding [20].

In laser welding, where energy density and cooling rates are very high, if compared to traditional arc one, and no filler material is used, the optimal source and the relating process parameters must be selected very carefully in order to achieve the optimum trade-off useful for obtaining a sound joint [21-22]. In this direction, this study aims to perform butt joint welding on high-strength low alloy steel materials with Fiber YAG laser, and to optimize the main processing parameters; laser power, welding speed and defocusing distance. Then, the tensile strength and the microhardness of the welds have been tested. Finally, the macro/ microstructure of the welds has been analyzed.

2. Experimental Work

The base material used in this study for welding was high strength low alloy steel sheets which were cut to size of 20 mm, 50 mm from 3 mm thick sheet. The chemical compositions and the mechanical properties of the base materials are provided in Tables 1 and 2, respectively. Prior to laser welding, the sample edges were ground to maintain positional accuracy and cleaned with fresh stainless wire brush followed by acetone swabbing, and then dried in the air. Welding was done as a butt joint perpendicular to the rolling direction of the sheets using a 3 kW YAG Fiber laser system. Welding was performed with a head angle of 00. Pure argon gas with a side nozzle at 15 L/min flow rate was used to protect the molten weld pool. To investigate the effect of the welding parameters on the macroscopic geometry, microstructure and mechanical properties of the joints, the welds were manufactured at various values of laser power, laser power, and defocusing distance. Three level of the laser power were investigated: 2500 W, 2000 W and 1500 W, at fixed welding speed of 40 mm/s and defocusing distance of -2 mm. Welding speeds of 50 mm/s, 40 mm/s and 25 mm/s were used at a fixed power of 2500 W and defocusing distance of -2 mm. Moreover, the defocusing distance was changed from -2 mm to +1.5 mm at a fixed power of 2500 W and welding speed of 40 mm/s. The welding conditions used for experimentation are summarized in Table 3.

The metallographic samples for the macro/ microstructural examination were cut from the weld cross-section, then mounted, ground, polished, and etched with a 2% Nital solution, to study the macroscopic weld geometry, microstructure of the weld and heat affected zone and observe the expected defects in the weld joints using a light microscope. The micro-Vickers hardness survey in the welded joint was conducted across the weld beads of the welded coupons employing Vickers micro-hardness testing machine with an indentation load of 9.8 N and loading time 15s at room temperature.

Tensile test was performed on samples that sectioned from the welded joint perpendicular to the welding direction. The test coupons were machined in such a way that the weld was positioned at the center of gauge length. Tensile tests were conducted using a fully computerized universal tensile testing machine at room temperature and with a strain rate of 5 mm/s. In each condition, three specimens have been tested and the average tensile strength of three results is obtained.

Table 1. Chemical compositions of the base metal, wt%

C	Si	Mn	P	S	Cr	Ni	Mo	V	Al	Fe
0.08	0.25	0.81	0.014	0.005	0.014	0.014	0.0008	0.003	0.05	Bal.

Table 2. Mechanical properties of the base metal

Yield Strength, MPa	Ultimate Tensile Strength, MPa	Elongation, %	Hardness, HV
335	422	22	161

Table 3. Welding conditions used for experimentation

Specimen No.	Power, W	Speed, mm/s	Defocusing distance, mm
# 1	2500	40	-2
# 2	2000	40	-2
# 3	1500	40	-2
# 4	2500	50	-2
# 5	2500	25	-2
# 6	2500	40	-0.5
# 7	2500	40	+ 0.5
# 8	2500	40	+1.5

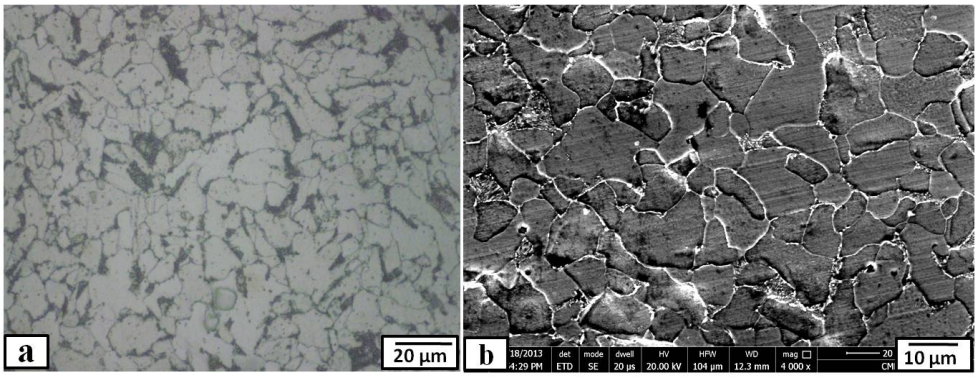

Figure 1. Microstructure of the base metal

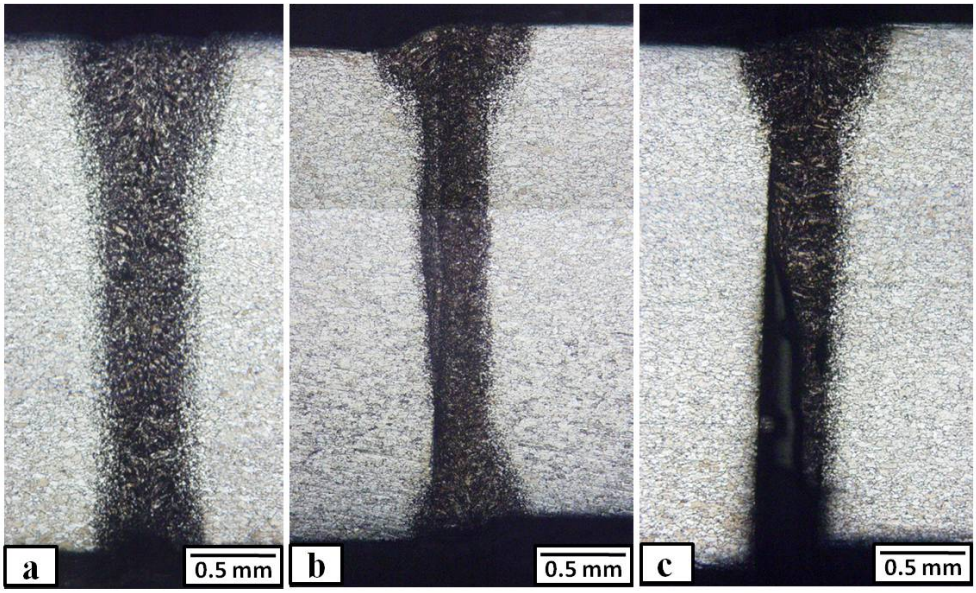

Figure 2. Macrographs of the weld cross-sections at different laser power, where (a) 2500 W, (b) 2000 W, and (c) 1500 W

3. Results and Discussions

3.1. Effect of Laser Welding Power

The microstructures of the HSLA steel base metals used in this work are shown in Fig. 1. The structure was characterized mainly by fine-grained polygonal ferrite (light etching) interspersed with grains of pearlite (dark-etching) structure. The representative weld joint cross-sections macrographs of samples welded at different weld powers (2500 W, 2000 W, and 1500 W) at fixed welding speed of 40 mm/s and defocusing distance of -2 mm are shown in Fig. 2. As can be seen in all conditions, the laser weld joint had a typical "goblet" shape that had a relatively wide zone at the upper surface and narrow nether zone at the rest of the thickness. The width of weld joint was slightly decreased by decreasing the welding power. At power of 2500 W, the width was 0.59 mm, and that 2000 W was 0.45 mm. For the power of 1500 W, the width became 0.42 mm. These data were measured at almost the center of the weld thickness. At laser powers of 2500 W and 2000 W, full penetration joints were obtained without any macro- defects, such as pores and cracks. At lower laser power (1500 W); partial penetration was obtained (See Fig.2 (c)). The heat generated at this lower power was not enough to melt the full thickness of the sample. Microstructures of the weld and heat affected zone of the three joints are shown in Fig. 3. At laser power of 2500 W, as can be seen in Fig. 3 (a), the structure of the weld zone was consisting of acicular ferrite with interspersed bainite structure. This is due to the relatively slow cooling rate after melting by laser power of 2500 W. When the laser power was decreased to 2000 W (Fig. 3 (b)), the clear dendritic structure was appeared in the weld zone as a course columnar crystal that grew from the base metal interface towards the weld centreline (opposite to the direction of heat flow). This is due to the relatively fast cooling rate after lower heat input of 2000 W. The weld zone was consisted of predominately acicular ferrite with some bainite. At laser power of 1500 W, the structure of the weld zone was very fine due to the consequent high cooling rate (Fig. 3 (c)). The most probably structure of the weld zone after laser power of 1500 W was martensite and some ferrite as shown in a enlarged SEM micrograph in Fig. 4 (a). Regarding the heat affected zone as shown in Fig. 3 (d-f), the width of the HAZ remarkably decreased by decreasing the laser power. The HAZ is heated to a high temperature for a sufficient time and subjected to a

complex thermal cycle (sudden heating followed by rapid cooling) over a wide temperature range. As a consequence, the HAZ consists of a variety of complex graded microstructures including all those phases existing in both the parent metal and the fusion zone. The transition of the microstructure from the weld zone to the base metal is illustrated in Fig. 3 (d-f). Their structures were consisted of ferrite, and partially decomposed pearlite observed at the grain boundary at welding power of 2500 W (see Fig. 3 (d). At lower power (1500 W), the HAZ structure was consisted of fine grains of acicular ferrite and bainite near the weld zone and the grains were gradually enlarged and changed to ferrite and partially decomposed pearlite by moving towards the base metal as shown in Figs. 3 (f) and 4 (b).

Results of tensile tests of the all welded joints are summarized in Table 4. Compared to the base metal, the fracture strength of samples # 1 (2500 W) and # 2 (2000 W) was almost the same, and the fracture location was in the base metal. This is due to the full penetration of these samples and the absence of the macro defects. For the sample # 3 of power of 1500 W, the fracture strength was much lower than that of the base metal. This is due to the partial penetration of the weld joint after this lower power.

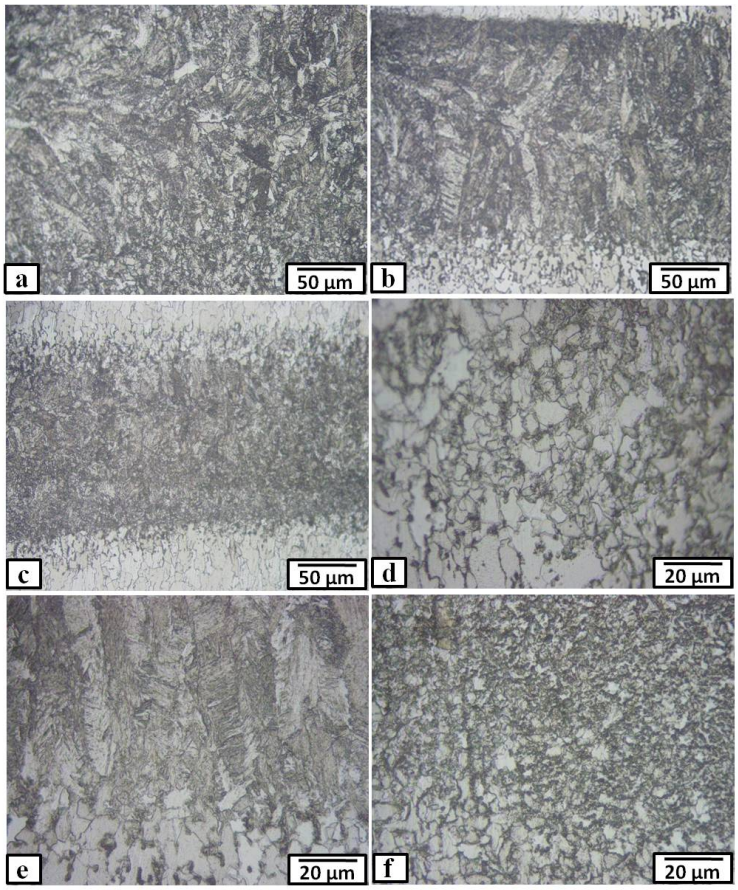

Figure 3. Microstructure of the weld zone (a-c) and heat affected zone (d-f) at different laser power, where (a) & (d) 2500 W, (b) & (e) 2000 W, and (c) & (f) 1500 W

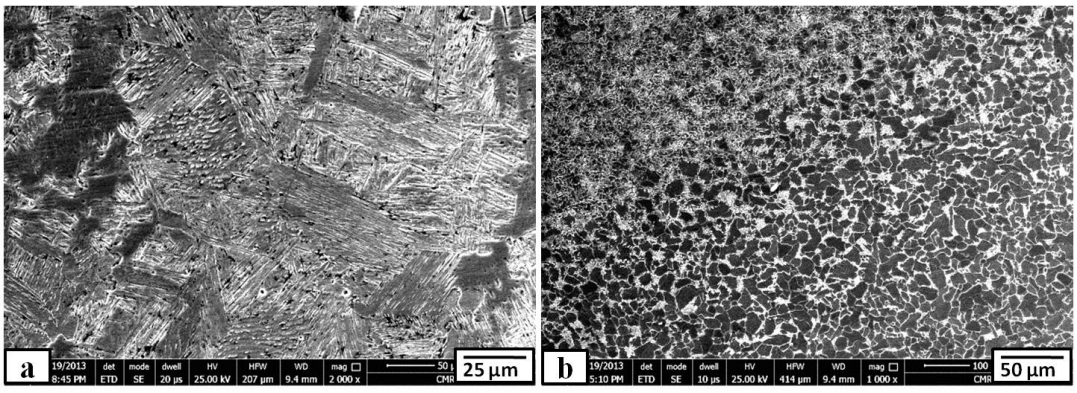

Figure 4. SEM micrographs of the (a) weld zone and (b) heat affected zone welded with laser power of 1500 W

Table 4. Tensile test results

No.	Power, W	Speed, mm/s	Defocusing distance, mm	Fracture Strength, MPa	Fracture location
# 1	2500	40	-2	424	Base metal
# 2	2000	40	-2	429	Base metal
# 3	1500	40	-2	331	Weld metal
# 4	2500	50	-2	422	Base metal
# 5	2500	25	-2	395	Weld metal
# 6	2500	40	-0.5	290	Weld metal
# 7	2500	40	+ 0.5	277	Weld metal
# 8	2500	40	+1.5	279	Weld metal

Figure 5 shows the hardness profiles through the cross-section perpendicularly to the welding direction of the three joints welded with different laser power. It is clear from this figure that the hardness values of the weld and heat affected zones in all joints were much higher than that of the base metal (161 HV). The reason for the significant hardness increment in the weld zone is result from the formation of hard phases such as martensite which is attributed to the higher cooling rate during solidification. Based on this explanation, the figure showed that the hardness in the heat affected zone and the weld metal becomes higher as the weld power becomes smaller.

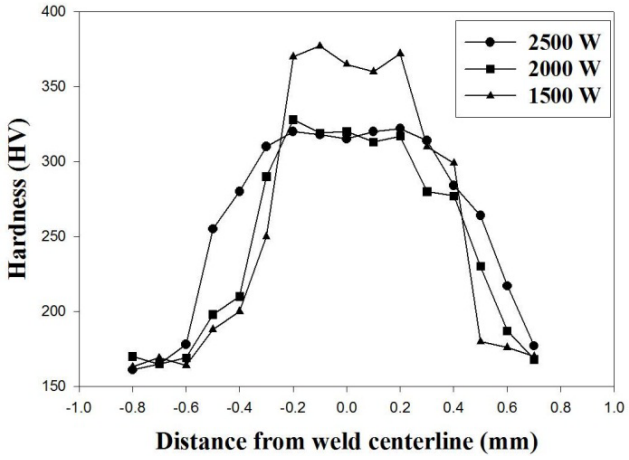

Figure 5. Hardness distribution through the cross-section perpendicularly to the welding direction of the three joints welded with different laser powers

3.2. Effect of Laser Welding Speed

Optical macrographs of the different weld cross-sections welded at different weld speeds (50 mm/s, 40 mm/s, and 25 mm/s) at fixed welding power of 2500 W and defocusing distance of -2 mm are shown in Fig. 6. It is clear from these figures that full penetration joints were obtained at all conditions in this part. This is due to the higher laser power (2500 W) that used. It can be seen also that cracks and porosities cannot be found in all condition. However, the changes in the welding speed show a clear influence on the weld width and consequently on the microstructure formation within the weld zone and heat affected zone. The width of the weld zone (measured in the mid of the thickness) of sample welded with speed of 50 mm/s (0.42 mm) and 40 mm/s (0.59 mm) was closer with each other. For the weld zone welded with speed of 25 mm/s, the width was much larger than those of other conditions. It reached to 1.1 mm. The amount of energy that is delivered to the work piece plays major role in the weld size and the microstructure. The used low welding speed (high heat-input) causes to the fusion pool longer residence in high temperature zone and slower cooling rate. This leads to enlarge the size of the weld zone. Regarding the weld microstructure, at welding speed of 50 mm/s as shown in Fig. 7 (a), the structure was consisted of ferrite and bainite. When the welding speed was reduced to half (25 mm/s), the structure showed large grains of ferrite and bainite as shown in Fig. 7 (c). For the heat affected zone, its structure was very similar to that of the laser power. As the heat input increased (through decreasing the laser speed), the cooling rate is decreased. In consequently, the width of the HAZ is increased. Moreover, the microstructure of the HAZ changed from ferrite and partially decomposed pearlite (Fig. 7 (d)) at higher speed of 50 mm/s to equiaxed ferrite-pearlite structure (Fig. 7 (f)).

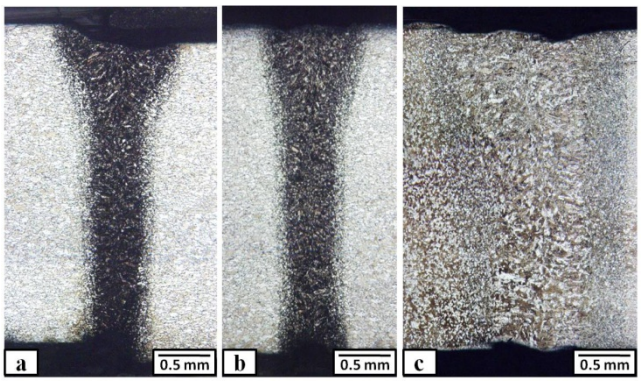

Figure 6. Macrographs of the weld cross-sections at different laser speed, where (a) 50 mm/s, (b) 40 mm/s, and (c) 25 mm/s

For the tensile test results, no significant differences were observed in the fracture strength of the samples welded with laser speed of 50 mm/s and 40 mm/s as shown in Table 4 (compare sample # 1 and 4). This is due to the similarity of the macro/microstructure obtained in both conditions. For the laser speed of 25 mm/s in sample # 5, the fracture strength decreased to 395 MPa. This is due to the softening of the weld and heat affected zones by the relatively lower cooling rate after welding with this condition.

The welding speed had a remarkable influence on hardness distribution both in weld and heat affected zones as shown in Fig. 8. The sample welded with laser speed of 25 mm/s showed lower hardness values. This variation in the hardness was due to the change of the metallurgical phase constituents after each condition. The lower hardness that was observed for sample welded with 25 mm/s, was inevitably the result of the relatively lower cooling rate combined with high energy density that promoted the formation of ferrite and bainite.

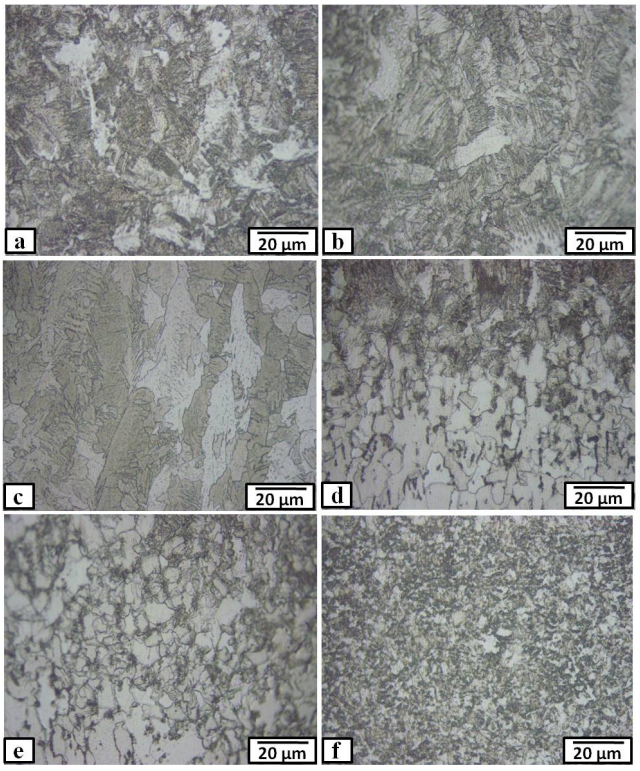

Figure 7. Microstructure of the weld zone (a-c) and heat affected zone (d-f) at different laser speed, where (a) & (d) 50 mm/s, (b) & (e) 40 mm/s, and (c)& (f) 25 mm/s

3.3. Effect of Defocusing Distance

Firstly, it is important to define the defocusing distance of the laser beam. It is the relative position of the laser beam focus and the sample surface. A negative defocusing distance is defined as the sample surface is above the laser beam focus, while a positive defocusing distance is defined as the sample surface is under the laser beam focus.

Fig. 9 shows the transverse welding cross-sections obtained at defocusing distance ranging from -2 mm to +1.5 mm at fixed laser power and speed of 2500W and 40 mm/s, respectively. It is clear from this figure that the width of the weld zone and HAZ increased with increasing defocusing distance. Moreover, the lack of penetration and other defects (porosity) were appeared at defocusing distance more than -1 mm, with the other process parameters held constant. This can be explained with concentration of the heat in each condition. At negative defocusing condition, the powder focus point and the powder concentration was below the molten pool; as a result, deeper materials will be melted. Similarly, when the defocusing distance is shifted to a more positive value, the laser focus point will be shifted to position above the molten pool. Based on this, more heat will be generated at the top surface, resulting in wide weld size in the top surface. This explanation was confirmed with the measured weld width as shown in Fig. 9. The weld width was 0.59 for defocusing distance of -2 mm. At defocusing distance of -0.5 mm, the width was 0.81 mm, and that + 0.5 mm was 0.89 mm. For the defocusing distance of +1.5 mm, the width became 0.99 mm. Moreover, there was inhomogenity in the microstructure of the weld and heat affected zones through the weld thickness at higher defocusing distance as shown in Fig. 10. Near the top surface, large grains were appeared due to lower cooling rate resulted from the more heat concentration in these areas. At the lower thickness portion, the weld zones were almost appeared as heat affected zone structure. The heat generated in these lower areas was not enough to melt of complete melt the faying edges of the two specimens.

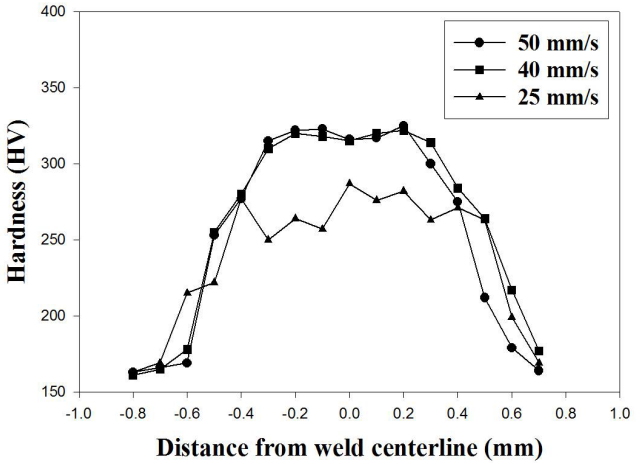

Figure 8. Hardness distribution through the cross-section perpendicularly to the welding direction of the three joints welded with different laser speeds

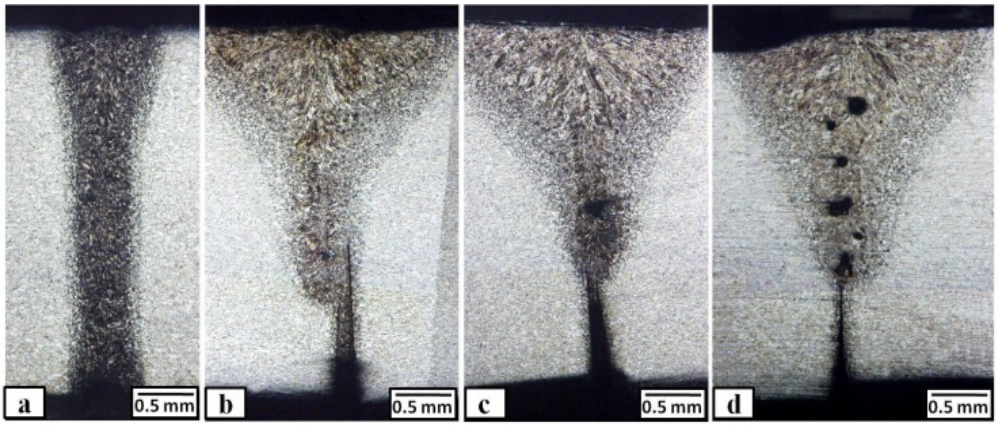

Figure 9. Macrographs of the weld cross-sections at different defocusing distance, where (a) – 2 mm, (b) – 1 mm, (c) +0.5 mm and (d) +1.5 mm

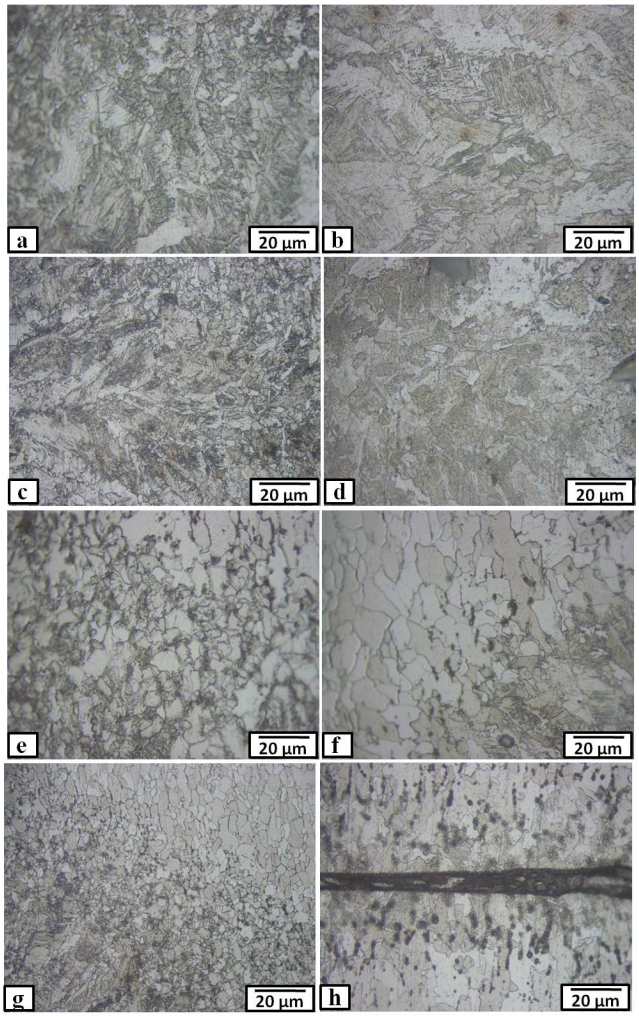

Figure 10. Microstructure of the weld zone (a-d) and heat affected zone (e-h) at different defocusing distance, where (a) & (e) – 2 mm, (b)&(f) – 1 mm, (c)&(g) +0.5 mm and (d)&(h) +1.5 mm

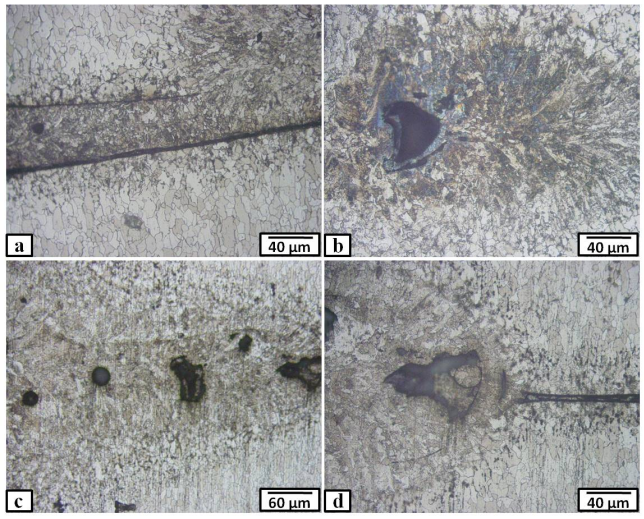

Figure 11. Microstructure of some defected areas in the weld zone welded with different defocusing distance, where (a) – 1 mm, (b) +0.5 mm , and (c) & (d) +1.5 mm

Regarding the appearance of some defects such as porosity at higher defocusing distance as shown in Figs. 9 (c-d) and 11, the laser keyhole becomes unstable and may readily collapse, leading to the formation of porosity at higher defocusing distance.

These macro/ microstructure variations inversely affect the strength of the welded joints. The samples of higher defocusing distance (# 6 – 8) showed lower fracture strength. The lack of penetration and other defects such as porosity decreases the sound thickness that can withstand the applied load, resulting in lowering the fracture strength of the welded joints.

4. Conclusions

In this work, high strength low alloy steel was welded using 3 kW YAG Fiber laser machine at different processing powers (2500, 2000, and 1500 W), laser speeds (50, 40 , and 25 mm/s), and defocusing distance (-2, -0.5, +0.5, and +1.5 mm). The macro/ microstructures of the weld and heat affected zones were investigated using optical and scanning electron microscopes. In addition, the fracture strength of the welded joints and hardness distribution through the cross-sections were evaluated. The results of this study led to the following conclusions:

- Full penetration joints without any macro defects were produced by laser processing power more than 2000 W. While at laser processing of 1500 W, partial penetration defect was occurred. The width of weld and heat affected zones was narrow at all processing powers. This is at fixed speed and defocusing distance of 40 mm/s and -2 mm, respectively.
- The laser speed has a remarkable effect on the width of weld and heat affected zones. As the welding speed decreases, their width is increased. The microstructure of the weld zone varies from acicular ferrite and bainite at lower speed to martensite and some ferrite at higher laser speed.
- The joint penetration and the weld zone width depend on the laser beam defocusing distance. Lack of penetration and other defects (porosity) with wide weld zone were appeared at defocusing distance more than -1 mm, with the other process parameters held constant.
- The fracture strength of the welded joints depends mainly of the welding power and defocusing distance. Close values to the base metal were achieved at higher laser powers and negative defocusing distance.

REFERENCES

[1] Xu W, Westerbaan D, Nayak S S, Chen D L, Goodwin F, Xu W, Westerbaan D, Nayak SS, Chen DL, Goodwin F, Zhou Y (2013) Tensile and fatigue properties of fiber laser welded high strength low alloy and DP980 dual-phase steel joints. Mater Des 43: 373–383.

[2] Shindell D, Faluvegi G, Walsh M, Anenberg SC, Dingenen RV, Muller NZ (2011) Climate, health, agricultural and

economic impacts of tighter vehicle-emission standards. Nat Clim Change 1: 59–66. doi:10.1038/nclimate1066.

[3] Hazratinezhad M, Arab NBM, Sufizadeh AR, Torkamany MJ (2012) Mechanical and metallurgical properties of pulsed neodymium-doped yttrium aluminum garnet laser welding of dual phase steels. Mater Des 33: 83–87.

[4] Li J, Nayak SS, Biro E, Panda SK, Goodwin F, Zhou Y (2013) Effects of weld line position and geometry on the formability of laser welded high strength low alloy and dual-phase steel blanks. Mater Des 52: 757–766.

[5] Ofioro J, Ranninger C (1997) Fatigue behaviour of laser welds of high-strength low alloy Steels. J Mater Process Technol 68 : 68-70.

[6] Shu Zhen, Zhenzhen Duan, Daqian Sun, Yexiong Li, Dandan Gao, Hongmei Li (2014) Study on microstructures and mechanical properties of laser–arc hybrid welded S355J2W+N steel. Opt Laser Technol 59: 11–18.

[7] Cao X, Wanjara P, Huang J, Munro C, Nolting A (2011) Hybrid fiber laser-arc welding of thick section high strength low alloy steel. Mater Des 32: 3399–3413..

[8] Saha DC, Westerbaan D, Nayak SS, Biro E, Gerlich AP, Zhou Y (2014) Microstructure-properties correlation in fiber laser welding of dual-phase and HSLA steels. Mater Sci Eng A 607: 445–453.

[9] Coelho RS, Corpas M, Moreto JA, Jahn A, Standfuß J, Kaysser-Pyzalla A, Pinto H (2013) Induction-assisted laser beam welding of a thermomechanically rolled HSLA S500MC steel: A microstructure and residual stress assessment. Mater Sci Eng A 578:125–133.

[10] Xizhang Chen, Yuanyuan Fang , Peng Li, Zhenzhen Yu, Xiaodong Wu, Dongsheng Li (2015) Microstructure, Residual Stress and Mechanical Properties of a High Strength Steel Weld using Low Transformation Temperature Welding Wires. Mater Des 65: 1214–1221.

[11] Wichan Chuaiphan, Loeshpahn Srijaroenpramong (2014) Effect of welding speed on microstructures, mechanical properties and corrosion behavior of GTA-welded AISI 201 stainless steel sheets. J Mater Process Technol 214: 402– 408.

[12] Jun Yan, Ming Gao, Xiaoyan Zeng (2010) Study on microstructure and mechanical properties of 304 stainless steel joints by TIG, laser and laser TIG hybrid welding. Opt Laser Technol 48: 512–517.

[13] Wu CS, Hu ZK, and Zhang YM (2009) Suppression of weld-bead defects and increase in the critical welding speed during high-speed arc welding. Proc Inst Mech Eng B, J Eng Manuf, 2009, Vol. 223, pp. 751–757. doi:10.1243/09544054JEM1369SC

[14] Catherine M Amodeo, Wei-Jen Lai, Jaewon Lee, Jwo Pan (2014) Failure Mode of Gas Metal Arc Welds in Lap Shear Specimens of High Strength Low Alloy (HSLA) Steel. Engineering Fracture Mechanics 131: 74–99.

[15] Rajashekhar S Sharma, Pal Molian (2011) Weldability of advanced high strength steels using an Yb:YAG disk laser. J Mater Process Technol 211: 1888– 1897.

[16] Parkes D, Westerbaan D, Nayak SS, Zhou Y, Goodwin F, Bhole S, Chen DL (2014) Tensile properties of fiber laser welded joints of high strength low alloy and dual-phase steels at warm and low temperatures. Mater Des 56: 193–199.

[17] Geng Li, Chen Zhang, Ming Gao, Xiaoyan Zeng (2014) Role of arc mode in laser-metal active gas arc hybrid welding of mild steel. Mater Des 61: 239–250.

[18] McDaniels RL, White SA, Liaw K, Chen L, McCay MH, Liaw PK (2008) Effects of a laser surface processing induced heat-affected zone on the fatigue behavior of AISI 4340 steel. Mater Sci Eng A 485: 500–507.

[19] Richardson DJ, Nilsson J, Clarkson WA (2010) High power fiber lasers: current status and future perspectives. J Opt Soc Am B 27: B63–B92.

[20] Mali Zhao, Tiegen Liu, Junfeng Jiang , Meng Wang (2014) Effect of defocusing distance on the contaminated surface of brass ring with nanosecond laser in a 3D laser scanning system. Opt Laser Eng 59: 11–18.

[21] Gangxian Zhu, Dichen Li, Anfeng Zhang, Gang Pi, and Yiping Tang (2012) The influence of laser and powder defocusing characteristics on the surface quality in laser direct metal deposition. Opt Laser Technol 44: 349–356.

[22] GAO Jin-qiang, QIN Guo-liang, YANG Jia-lin, HE Jian-guo, ZHANG Tao, WU Chuan-song (2011) Image processing of weld pool and keyhole in Nd:YAG laser welding of stainless steel based on visual sensing. Trans Nonferrous Met Soc China 21: 423-428.